JOURNAL OF MATERIALS SCIENCE 14 (1979) 2083–2090

Quantitative microstructural analysis of reaction-bonded silicon nitride

J. HEINRICH, G. STREB
DFVLR, Institut für Werkstoff-Forschung, Postfach 90 60 58, D-5000 Köln 90, West Germany

Quantitative analysis of the essential microstructural parameters of injection-moulded reaction-bonded silicon nitride was performed. The effect of silicon grain size on the porosity, the pore size distribution, the degree of reaction and the proportions of the alpha and beta modifications and the grain size of these phases was studied under constant processing conditions. With increasing silicon grain size the degree of reaction and the total porosity and density remain unaffected. The percentage of beta phase, the grain size of alpha and beta modifications as well as the mean pore diameter increase with increasing grain size of the starting powders. The effect of the structural parameters on the room-temperature strength is discussed.

1. Introduction

Owing to its favourable high-temperature characteristics silicon nitride is considered to be a suitable material to replace superalloys for the construction of small gas turbines. The mechanical properties of silicon nitride, such as flexural strength, creep behaviour and thermal shock resistance, are essentially determined by the type and distribution of the microstructural constituents and the physical properties, such as Young's modulus and thermal conductivity. Usually variation of processing conditions results in changes in various microstructural parameters [1, 2].

The structural morphology of reaction-bonded silicon nitride (RBSN) is characterized by the proportions of the alpha and beta modifications, grain-size distribution, total porosity, pore-size distribution and unreacted silicon. Only a few investigations concerning the interdependence of quantitatively determined microstructural parameters and mechanical properties of RBSN have been performed, and some of the results and interpretations are contradictory [3–7].

The present investigation is concerned with the study of the microstructural parameters of RBSN. The room-temperature flexural strength of the material investigated is discussed as a function of these parameters.

2. Experimental details

Quantitative characterization of a multiphase microstructure requires determination of the number of phases and overall stereometric parameters, such as volume percentage of these phases. In this paper, the porosity is considered as a separate phase. Additional parameters to be considered are the geometrical arrangement of the individual phases relative to the particle size and shape and deviation from statistical distribution [8]. A quantitative analysis will be performed using two RBSN materials.

2.1. Sample preparation

The two different types of RBSN investigated were prepared from silicon powders of different grain size. The grain-size distribution, specific surface area, and chemical analysis are shown in Fig. 1 and Table I.

The powders were injection-moulded to the same green density ($\rho = 1.50\,g\,cm^{-3}$). These specimens were nitrided for 100 h in a furnace with a stainless steel chamber having molybdenum heating

0022–2461/79/092083–08 $02.80/0

TABLE I Characteristics of the silicon powders

	A	B
Grain size*	< 10	37–63
d at 50% weight fraction (Fig. 1) (μm)	7	51
B. E. T. surface area [$m^2\ g^{-1}$]	2.09	0.24
Impurity element content (wt %)		
iron	0.58	0.8
aluminium	0.17	0.16
calcium	0.02	0.02
carbon	0.04	0.05
oxygen	0.8	0.4

*Supplier values.

elements and radiation shields. A mixture of 90 vol % N_2 and 10 vol % H_2 was used under static conditions at a constant nitriding gas pressure of 950 mbar. The temperature–time programme and the course of reaction for both materials used is shown in Fig. 2.

The degree of reaction versus time was calculated from the consumption of nitrogen during nitridation. The total nitrogen consumption was in accordance with the degree of reaction, determined from the weight gain after the complete nitriding cycle (see Section 2.2) – more details of the processing conditions have been presented elsewhere [1]. The room temperature flexural strength of the nitrided specimens, dimensions 3.5 mm × 4.5 mm × 45 mm, was determined by the four-point bend test method.

2.2. Degree of reaction

The theoretical weight increase due to complete reaction of silicon to silicon nitride according to

$$3Si_{(s)} + 2N_{2\,(g)} \rightleftharpoons Si_3N_{4(s)} \qquad (1)$$

is 66.49%. The degree of reaction (DR) is thus determined by the ratio

$$DR = \frac{\text{observed weight increase}}{\text{theoretical weight increase}}. \qquad (2)$$

The error in determining the degree of reaction is due to the amount of free silicon (m_1) and to losses of material due to evaporation of silicon during nitridation (m_2), so that a negative correction term to DR is obtained (m_3 = specimen mass prior to reaction).

$$DR = 1 - \frac{0.66\,m_1 + 1.66\,m_2}{0.66\,m_3}. \qquad (3a)$$

In volume per cent, V_v, the degree of reaction is calculated as follows:

$$DR = 1 - [V_v(1) + 2.5\,V_v(2)] < 1. \qquad (3b)$$

If the grain size of the silicon powder decreases, the evaporation rate of silicon increases due to the larger specific surface area and the degree of reaction decreases (Table II). At a degree of reaction

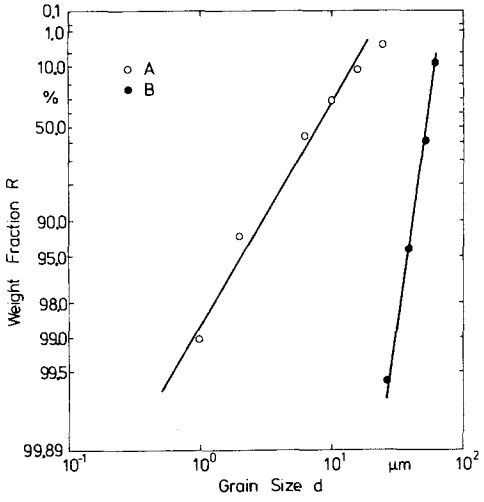

Figure 1 Grain-size distribution of the silicon powders.

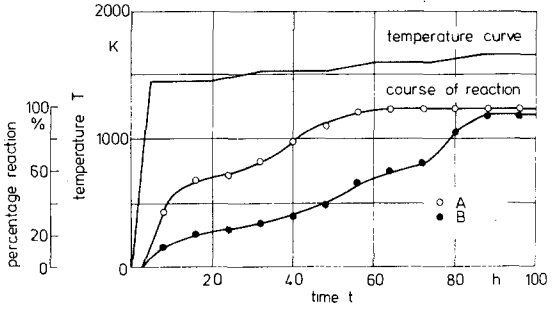

Figure 2 Course of reaction during nitridation.

TABLE II Microstructural parameters of the two RBSN materials

Parameter	Material	
	A	B
Degree of reaction (%)	89.9	93.0
Unreacted silicon (vol %)	$\leqslant 4$	$\leqslant 4$
Density ($g\,cm^{-3}$)	2.41	2.38
α-phase $\alpha/\alpha+\beta$ (%)	82	60
α/V_0 (%)	62	45
β-phase $\beta/\alpha+\beta$ (%)	18	40
β/V_0 (%)	13.6	30
Total porosity (calculated) (vol %)	24.2	25.2
Total porosity (from optical micrographs) (vol %)	22	25
Open porosity (vol %)	17	10.8
Pore openings (vol %)	5.1	1.3
Micropores $d^*_{min} < d_h < d^*_{max}$ (μm)	$0.012 < 0.073 < 0.2$	$0.037 < 0.185 < 0.47$
Macropores $d^*_{min} < d_h < d^*_{max}$ (μm)	$1 < 1.5 < 10$	$1 < 10 < 50$
α-grain size, length (μm)	0.5	0.7
width (μm)	0.1	0.1
β-grain size (μm)	0.5	3

*d-values at a relative frequency of about 1%.

of 90% and a proportion of free silicon of about 4% ($V_v(1)$) (see Table II) the volume percentage of evaporated silicon is 2.4% ($V_v(2)$).

2.3. Density and total porosity

At equal green density and similar degree of reaction, the densities determined according to Archimedes' principle and the total porosities (calculated from density) are approximately the same for materials prepared from silicon powders of different grain size (Table II). The observed overall density is proportional to the volume percentages and the densities of the phases.

$$\rho = \sum \frac{V_\nu \cdot \rho_\nu}{V_0} \tag{4}$$

where V_ν is the volume of the various phases, V_0 the total volume of the specimen, and ρ_ν the density of the various phases.

When the total porosity is calculated from the density, unreacted silicon ($\rho = 2.33\,g\,cm^{-3}$) has to be taken into account as solid phase in addition to Si_3N_4 ($\rho = 3.18\,g\,cm^{-3}$).

$$V_v(P) = 1 - \frac{\rho_{\text{as-measured}}}{\rho_{Si_3N_4}} - V_v(Si)\left(1 - \frac{\rho_{Si}}{\rho_{Si_3N_4}}\right)$$

where $V_v(P)$ is the volume percentage of the pores, and $V_v(Si)$ the volume percentage of unreacted silicon. At a proportion of unreacted silicon amounting to 4% (see Table II) the value for the correction term $V_v(Si)\,(1 - \rho_{Si}/\rho_{Si_3N_4})$ is within the measuring accuracy of 1%.

*Erba Science Company, Milan, Italy.

2.4. X-ray analysis

Powder fractions $d < 63\,\mu m$ were investigated by standard powder diffraction using Cu$K\alpha$ radiation. The ratio

$$F = \frac{I_{\beta(101)} + I_{\beta(210)}}{I_{\alpha(102)} + I_{\alpha(210)}} \tag{6}$$

was determined. From a calibration curve the relative volume percentage of a phase per total amount of Si_3N_4 can be given [9].

In material A, the volume percentage of the alpha phase is found to be 37.8% greater than in material B (Table II). The reason for this is due to the different silicon grain size of the starting powder (Table I). In material A, the evaporation rate of silicon is higher as a result of the greater specific surface area. Since the alpha phase is probably formed by a gas-phase reaction between Si and/or SiO and N_2 [4, 10–13], a higher volume percentage of the alpha phase is expected at constant green density with increasing specific surface area (see [15–17]).

2.5. Pore-size distributions

2.5.1. Mercury pressure porosimetry

The volume fraction of the open porosity and its pore-size distribution in the range $d \leqslant 15\,\mu m$ were determined by mercury pressure porosimetry*. The surface tension, σ, of mercury, the wetting angle θ, between Si_3N_4 and Hg, and the hydrostatic pressure of mercury are correlated to a

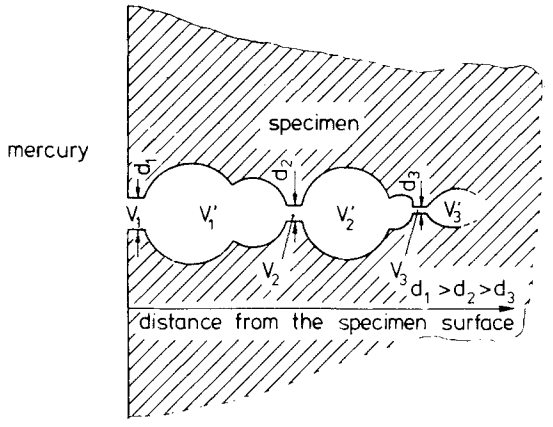

Figure 3 Arrangement of a bottle-shaped pore (schematic).

penetrable cylindrical pore diameter following Equation 7.

$$d = -\frac{4}{p}\sigma \cos\theta \qquad (7)$$

with $\sigma = 480\ \mathrm{MN\,m^{-1}}$ and $\theta = 141.3°$.

Generally, porous ceramic materials contain bottle-shaped pores rather than cylindrical ones (Fig. 3). At a pressure p_1 and a correlated diameter d_1 the volume V_1 of the pore-opening channel and the volume V_1' of the pore will be filled with mercury until pore openings with $d_2 < d_1$ are reached (Fig. 3). At higher pressures, $p_1 < p_2 < p_3$, the same scheme is valid for smaller pore-opening diameters $d_3 < d_2 < d_1$. If the pressure is decreased, the pore volumes V_1', V_2', and V_3' remained filled. Repeating the test, only the diameters and volumes of the pore-opening channels are measured (hysteresis). Therefore, using this technique, the distribution of pore-opening diameters can be determined but not the actual distribution of the diameters of the open pores themselves.

At a given pressure p_1 the spatial distribution of the pore opening diameters d_1 determines the penetration depth of mercury into the sample. Therefore, with large samples and/or low pressures only pore volumes close to the surface may be measured. All pores in the rest of the volume with pore-opening diameters d_1 are measured at higher pressures. This leads to an apparent increase of small pore openings and the distribution function, showing the volume fraction $\Delta V/V_p$ (V_p = total penetrated Hg-volume) per class width Δd as a function of the pore-opening diameter, becomes asymmetric, as shown in Fig. 4 (thickness of the sample = 3.5 mm). In order to obtain realistic distribution curves of the pore opening diameters the samples had to be thinned to 1.1 mm (further thinning of samples did not result in changes of the distribution curves).

The hysteresis curves show approximately the same shape as the distribution functions in the case of thin specimens ($h \leqslant 1.1$ mm, Fig. 4). This means that in each Δd interval the ratio of the pore volume V' to the volume of the corresponding pore-opening channel V is constant (see Fig. 3). Consequently, the diameter d_h (Table II) corresponding to the maximum of the distribution curve ($h \leqslant 1.1$, hysteresis) is representative of the pore-opening diameter which contributes most to the pore-opening volume of the sample.

With increasing silicon powder grain size the distribution functions of the pore-opening diameters (micropores) are shifted towards larger d-values (Fig. 4). Fig. 8a and b (Section 2.6) show that the size of these micropores is comparable with the pores inside the α-matte. For both materials, A and B, the value of the total open porosity was independent of the specimen dimensions. With increasing silicon powder grain size, the volume percentage of the open porosity and the percentage of the micropores, calculated from hysteresis curves, decrease.

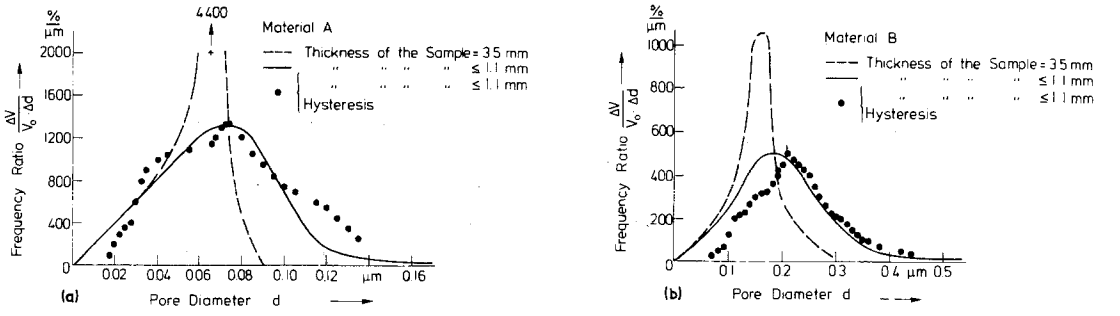

Figure 4 Pore-size distribution of the micropores: (a) material A, (b) material B.

In spite of the problems of this test method the distribution of the micropores yields a valid parameter characterizing some properties of RBSN, such as oxidation behaviour, because the micropores are responsible for the SiO_2 surface-layer formation. As an example, material A with smaller micropores exhibits considerably better oxidation behaviour than material B [18].

2.5.2. Optical microscopy

Owing to the different reflectivity of the individual phases, Si_3N_4, Si and pores can be distinguished by optical microscopy (Fig. 5).

The volume percentages V_v of the phases were determined from scanning optical micrographs using the following relation:

$$V_v = \frac{L_\nu}{L_0} \tag{8}$$

where L_ν is the length in the ν phase, and L_0 the test length. The proportion of unreacted silicon is constant in both materials (Table II). The mean particle size is 2.5 μm in material A and 3.5 μm in material B. In both materials inhomogeneous distribution of unreacted silicon is observed (Fig. 6). The volume percentage of the pores determined by optical microscopy (Table II) is due to the proportions of the closed and open pores with $d \geqslant 1\,\mu$m and preparation errors.

An assessment of the preparation error was not possible, since the ratio of the proportions of pores with $d \geqslant 1\,\mu$m and $d \leqslant 1\,\mu$m could not be determined by the measuring techniques employed. It was only possible to specify the sum of the proportions for the open and closed porosity. Assuming that the proportion of pores with $d < 1\,\mu$m is negligible, the minimum preparation error amounts to 3% for material A and 1% for material B.

The accumulation of small pores visible in some areas of Fig. 6 may represent intersections of serrated and fissured larger pores. The areas of the pores in polished sections (macropores) have been determined by a half automatic structure analyser*. Fig. 7 shows the area fraction $\Delta A/A_0$ (A_0 = total pore area) per class width Δd as a function of the pore diameter. With decreasing initial grain size of the silicon starting powder, i.e. with decreasing pore size in the green state, the total distribution curve of the macropores is shifted towards smaller d-values (see Table II).

2.6. Scanning electron microscopy

The grain size of RBSN was determined using etched microsections. The alpha and beta modifications can be distinguished due to their different grain shape and grain size. The equi-axed beta crystallites were etched by chemical etching (NaOH melt at 673 K, 40 sec) and the alpha whiskers by ion bombardment (argon ions, 3 h) (Fig. 8).

The alpha phase is formed by a gas-phase reaction [4, 10–13] which occurs in whisker-shaped crystallites (alpha matte) (Fig. 8a and b). The alpha Si_3N_4 formation continues until either reaction partner, gaseous Si or SiO and N_2, is no longer available. The reaction ceases when the pores close thus blocking the supply of nitrogen or when, as a result of the formation of a surface

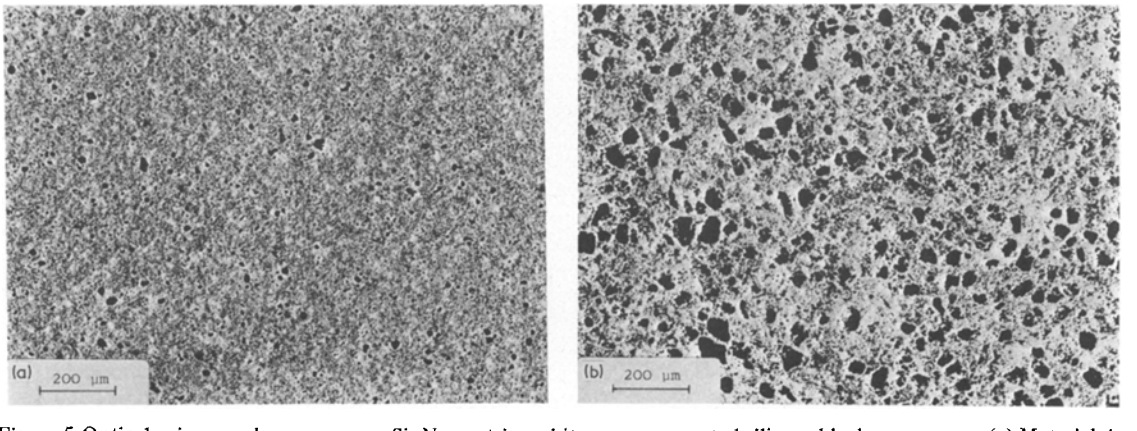

Figure 5 Optical micrographs: grey area, Si_3N_4 matrix; white area, unreacted silicon; black area, pores. (a) Material A, (b) material B.

*Type MOP, Kontron Company, Eching, West Germany.

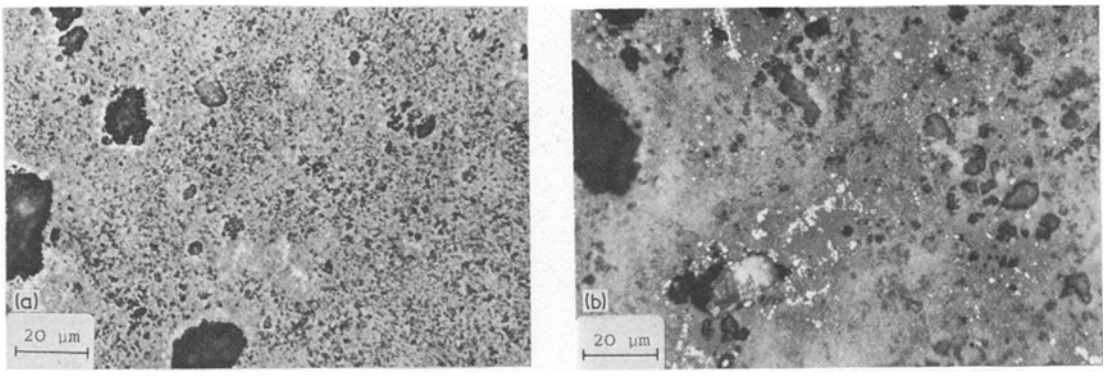

Figure 6 Optical micrographs: white area, unreacted silicon. (a) Material A, (b) material B.

layer, gaseous Si (and/or SiO) is no longer present.

After the nitridation, approximately 50% of the total porosity is open porosity. Hence it can be assumed that the formation of the surface layer prevents the formation of alpha. Growth is impeded when the α-needles interfere with each other or when a gaseous reaction partner is no longer available. The pores in material B are larger than in material A; as a result larger alpha whiskers are formed in material B (Table II). Owing to the smaller crystallite size, the distribution of the newly formed micropores in the alpha phase is shifted towards smaller d-values in material A (Fig. 4).

At nitridation temperatures below 1400° C, the beta phase is formed by diffusion of nitrogen to the Si–Si_3N_4 interface where reaction occurs [13, 14]. The grain size of the equi-axed beta grains increases with increasing initial Si grain size (Fig. 8c and d; Table II). Since a Si powder grain may consist of several crystallites and since the grains shrink during the alpha formation, the existing beta crystals may be smaller than the initial grain size, in spite of the expansion during nitridation.

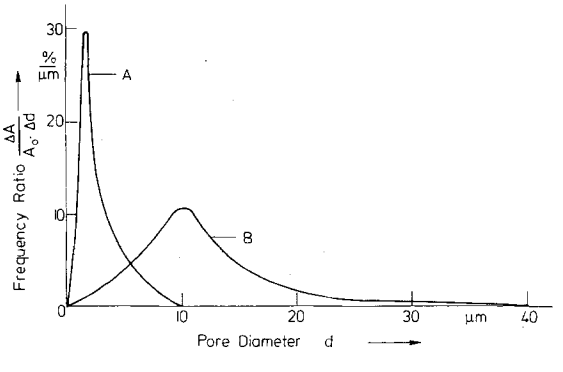

Figure 7 Pore-size distributions of the macropores.

3. Discussion

The relationship between the strength of the nitrided specimens (four-point bend test: A, 218 MN m^{-2}; B, 150 MN m^{-2}) and the individual structural parameters can only be of a qualtitative nature within the scope of this paper since they have been related by only two test values. Apparently the percentage of the open porosity is not a suitable parameter to describe changes in strength. Without any influence on the total porosity and on the alpha/beta ratio, the closed porosity can be transformed into open porosity by annealing and there is no appreciable change in room-temperature strength [18].

According to Griffith's equation (Equation 9) for the critical stress, the grain and pore diameter are to be regarded as the critical crack sizes,

$$\sigma_f = \sqrt{\left(\frac{E \cdot \gamma}{\pi \cdot C}\right)} \qquad (9)$$

where σ_f is the critical stress, E Young's modulus, γ the surface energy, and C the critical crack size. The grain size and the pore diameter decrease in material A, while the strength is increased by 38%. (A silicon powder with an intermediate grain size, 10 to 37 μm, gives intermediate strength [2]). From these results, however, it cannot be decided to what degree grain size and pore diameter contribute to this increase.

There are also indications in the literature that show that it is not possible to consider the strength only as a function of one structural parameter since owing to variations of the manufacturing conditions the influence of other strength-controlling factors cannot be excluded. For example, Elias *et al.* [4] and Jennings *et al.* [3] always relate the materials low flexural strength to high beta percentages, whereas Mangels and Cassidy [5] do not

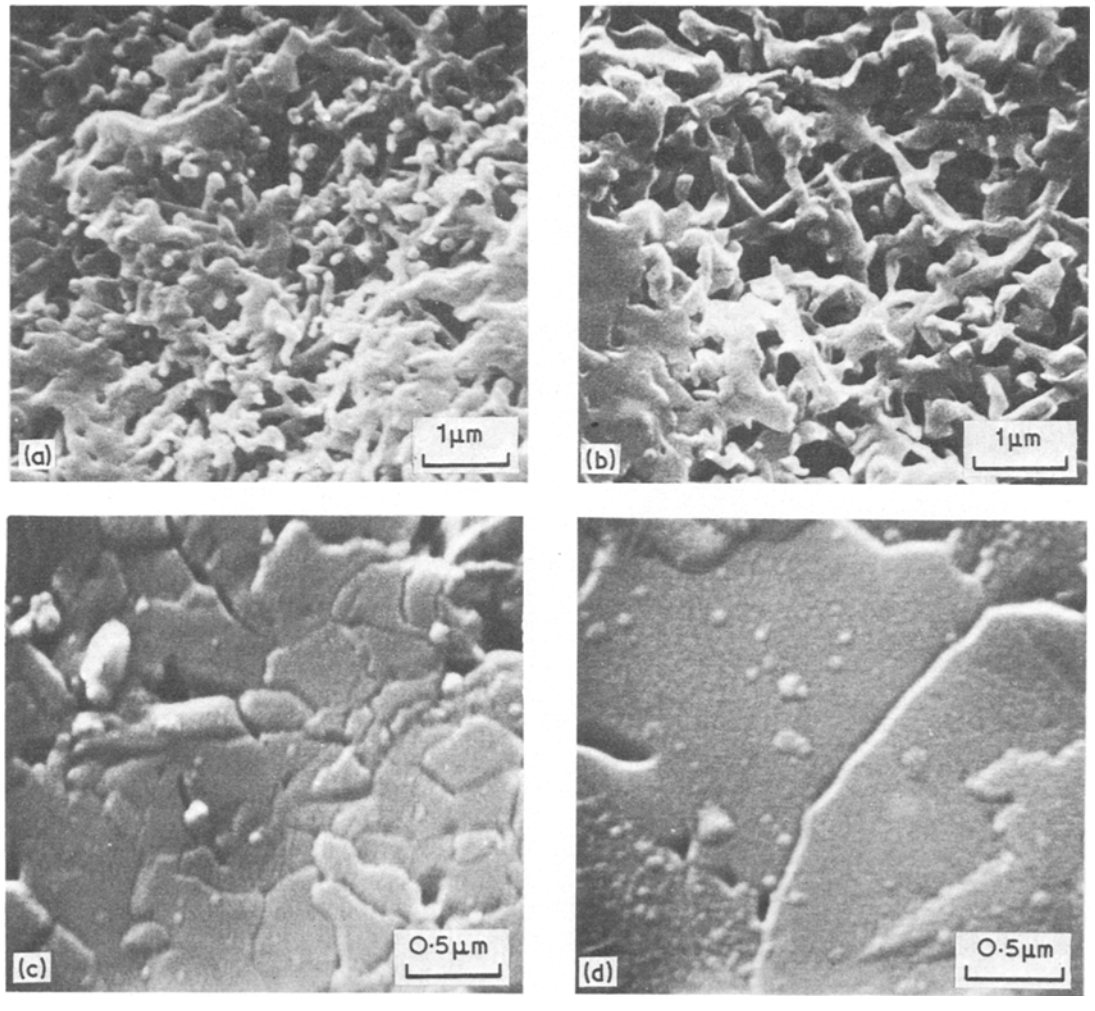

Figure 8 Scanning electron micrographs. (a) and (b) α-phase in material A and B. (c) and (d) β-phase in material A and B.

observe any effect of the alpha/beta ratio on the flexural strength.

The objective of further activities is, therefore, to separate the influence of the alpha/beta ratio and the pore diameter by means of an appropriate variation of the manufacturing conditions.

4. Conclusions

Two silcon powders with different grain-size distributions were injection-moulded to the same green density. After nitriding to a degree of reaction of about 90% the following structural changes have been observed. With decreasing silicon powder grain size

(1) the density and thus the total porosity and the proportion of unreacted silicon are not affected;

(2) the percentage of the open porosity increases;

(3) the percentage of the alpha modification increases;

(4) both the diameter of the newly formed micropores in the alpha phase and the diameter of the macropores decrease;

(5) the grain sizes of the alpha and beta crystallites decrease; and

(6) the flexural strength increases.

Acknowledgements

The authors wish to acknowledge helpful discussions with Professor Dr H. Hausner, and the financial support given by the Deutsche Forschungsgemeinschaft (D-5300 Bonn-Bad Godesberg 1, Kennedy Allee 40).

References

1. J. HEINRICH and M. BOHMER, Forschungsbericht der Deutschen Luft- und Raumfahrt DLR-FB 77-22 (1977).
2. J. HEINRICH, *Ber. Dt. Keram. Ges.* **55** (1978) 238.
3. H. M. JENNINGS, S. C. DANFORTH and M. H. RICHMAN, in Proceedings of the Second International Conference on Mechanical Behaviour of Materials, Boston (1976) p. 1877.
4. D. P. ELIAS, B. F. JONES and M. W. LINDLEY, *Powder Met. Int.* **8** (1976) 162.
5. J. A. MANGELS and D. J. CASSIDY, "Physical Properties of Injection Molded Silicon Nitride", Presented at the Meeting of the American Ceramic Society, Cincinnati (1973).
6. R. W. RICE, *J. Mater. Sci.* **12** (1977) 627.
7. B. F. JONES and M. W. LINDLEY, *ibid* **12** (1977) 630.
8. G. ONDRACEK, *Sci. Ceram.* **6** (1973) III 3–44.
9. H. KNOCH, R. LEUCHT and G. ZIEGLER, *Sonderbände der Praktischen Metallographie* **9** (1979) 255.
10. D. R. MESSIER and P. WONG, *J. Amer. Ceram. Soc.* **56** (1973) 480.
11. D. CAMPOS-LORIZ and F. L. RILEY, *J. Mater. Sci.* **11** (1976) 195.
12. F. L. RILEY, Proceedings "Nitrogen Ceramics", edited by F. L. Riley, Nato Advances Study Institutes Applied Science Series no 23, Noordhoff International Publ. BV (1977) 265–88.
13. H. M. JENNINGS and M. H. RICHMAN, *J. Mater. Sci.* **11** (1976) 2087.
14. P. LONGLAND and A. J. MOULSON, *ibid* **13** (1978) 2279.
15. S. WILD, P. GRIEVESON and K. H. JACK, *Special Ceramics* **5** (1972) 385.
16. I. AMATO, D. MARTORANA and M. ROSSI, *Powder Met.* **18** (1975) 339.
17. D. CAMPOS-LORIZ and F. L. RILEY, *Sci. Ceram.* **9** (1977) 38.
18. J. HEINRICH, unpublished work.

Received 25 September 1978 and accepted 22 January 1979.